Fuel 420 (2026) 138968

Contents lists available at ScienceDirect

Fuel

journal homepage: www.elsevier.com/locate/jfue

Full length article

Analysis of $CH_2O \cdot OH$ as marker for the heat release rate from air to pure oxy-fuel flames at elevated preheat temperature, pressure and strain

Björn Stelzner[a,*], Peter Habisreuther[a], Fabian P. Hagen[a], Matthias M. Sentko[a], George Vourliotakis[b], Christos Keramiotis[b], Maria Founti[b], Dimosthenis Trimis[a]

[a] Karlsruhe Institute of Technology (KIT), Engler-Bunte-Institute, Combustion Technology, Karlsruhe, Germany
[b] Laboratory of Heterogeneous Mixtures and Combustion Systems, School of Mechanical Engineering, NTU of Athens, Zografou, Greece

HIGHLIGHTS

- CH_2O·OH confirms as robust HRR marker across a wide range of conditions including variations in oxidizer content, equivalence ratio, preheat temperature, pressure, and strain.
- For CH_4-air flames, the highest correlation between CH_2O·OH and HRR occurs at slightly rich mixtures ($\Phi \approx 1.5$), while in CH_4/O_2 flames, the strongest correlation shifts to ultra-rich conditions ($\Phi \approx 3.0$).
- Elevated pressure generally improves the correlation at leaner mixtures but narrows the range of high correlation, whereas preheating shifts the optimal equivalence ratio to richer conditions and broadens the applicability range.
- Even under high strain rates (up to 10,000 s^{-1}, relevant for turbulent flames), CH_2O·OH maintains a strong correlation ($R \approx 0.9$) with HRR, highlighting its suitability for turbulent combustion diagnostics.
- The results of this study are intended to support and guide experimental diagnostics by identifying reliable marker regimes.

ARTICLE INFO

Keywords:
Heat release rate
$CH_2O \cdot OH$
Formaldehyde
Hydroxyl radical
Premixed flames
Oxy-fuel

ABSTRACT

This work presents a numerical investigation of the applicability of the product of formaldehyde (CH_2O) and hydroxyl radicals (OH), denoted as $CH_2O \cdot OH$, as a marker for the local heat release rate (HRR) in CH_4 flames over a broad range of boundary conditions. Both laminar freely propagating one-dimensional and premixed counterflow CH_4 flames were simulated using several detailed reaction mechanisms. The analysis systematically varied the oxidizer composition (from air to pure oxy-fuel), equivalence ratio (Φ), inlet temperature, pressure, and strain rate. The correlation between the $CH_2O \cdot OH$ profiles and the HRR was quantified using the Pearson correlation coefficient. Overall, the study confirms $CH_2O \cdot OH$ as a practical and reliable HRR marker in CH_4 flames, particularly under high-temperature and high-pressure oxy-fuel conditions. The results show that in slightly rich CH_4-air flames (about $\Phi = 1.5$), $CH_2O \cdot OH$ provides an accurate estimate of the HRR. In oxygen-enriched and pure oxy-fuel flames, the strongest correlation shifts to ultra-rich conditions (about $\Phi \approx 3.0$). Increasing pressure enhances the correlation at lower equivalence ratios, whereas preheating weakens the correlation locally but expands the overall range of validity. Although increasing strain rate generally degrades the correlation, $CH_2O \cdot OH$ remains a robust marker under technically relevant turbulent conditions (strain rates below 10,000 s^{-1}), maintaining Pearson correlation coefficients of approximately $R \approx 0.9$ even close to extinction. This demonstrates the strong feasibility of using $CH_2O \cdot OH$ for HRR estimation in highly turbulent flames. The demonstrated robustness of $CH_2O \cdot OH$ highlights its suitability as an HRR marker, providing valuable insights for experimental diagnostics.

1. Introduction

The local heat release rate (HRR) is a key factor in determining the flame structure and dynamics, and it provides important insights into the chemical time scale in combustion processes. Since HRR cannot be measured directly, significant efforts have been devoted in previous studies to identifying experimentally accessible surrogate markers.

* Corresponding author.
Email address: bjoern.stelzner@kit.edu (B. Stelzner).

https://doi.org/10.1016/j.fuel.2026.138968
Received 30 July 2025; Received in revised form 18 December 2025; Accepted 28 February 2026
Available online 4 March 2026

Najm et al. [1] investigated several potential species as markers for measuring the flame burning rate. They found that CH, OH*, C_2*, and CH* are not reliable indicators for premixed methane–air V-flames, as these species are not directly involved in the primary carbon breakdown pathway, which proceeds as $CH_4 \rightarrow CH_3 \rightarrow CH_2O \rightarrow HCO \rightarrow CO \rightarrow CO_2$. In contrast, the formyl radical (HCO) was identified as a highly suitable marker, exhibiting a strong correlation with the local HRR across a wide range of flame curvatures and strain rates. Nevertheless, because the main contribution to heat release in hydrocarbon flames arises from the formation of H_2O and CO_2, HCO primarily reflects the forward conversion toward these final products rather than the total HRR.

The direct experimental measurement of HCO using planar laser-induced fluorescence (PLIF) was first demonstrated by Najm et al. [1], achieving a signal-to-noise ratio (SNR) of approximately 2:1 in frame-averaged images over 100 frames. Similarly, Jeffries et al. [2] reported an SNR of around 3:1 in CH_4/O_2 flames at an equivalence ratio (Φ = 1.03) and low pressure (5.8 torr). Kiefer et al. [3] obtained single-shot PLIF images with SNRs ranging from 6:1 to 12:1 in lean CH_4/O_2 flames. They later extended their study to turbulent premixed CH_4-air flames, proposing effective strategies for HCO detection [4]. Moreover, they recommended restricting HCO PLIF detection to lean or stoichiometric conditions, since larger hydrocarbons can significantly interfere with the inherently weak HCO signal. Additionally, they cautioned that excessively high laser pulse energies can induce artificial HCO formation via photolysis of CH_2O, limiting the benefit of simply increasing laser energy to enhance the signal.

To overcome these experimental challenges, Paul and Najm [5] introduced an alternative approach for HRR estimation in stoichiometric dimethyl ether/air flames. This method approximates the local HRR based on the simultaneous measurement of formaldehyde (CH_2O) and hydroxyl radical (OH), forming their scalar product. This product has been shown to correlate strongly with the HCO concentration, and thus with the local HRR. The experimental implementation of this technique has gained widespread use, as simultaneous detection of CH_2O and OH is feasible even in turbulent flames using laser-induced fluorescence (LIF) [6–9], including high-speed imaging modes [10,11]. Moreover, this approach has been successfully extended to flames involving higher hydrocarbons beyond CH_4, producing promising results [12,13], and has even been applied in dense spray flames [14]. Only a few studies have explored boundary cases in combustion. Kosaka et al. [15] applied the $CH_2O \cdot OH$ product technique to investigate flame–wall interactions in CH_4–air flames. Fan et al. [16] applied this approach to lean CH_4/H_2 swirling wall-impinging flames. In this study, in addition to clearly defined HRR zones along the flame front, a highly fragmented structure was observed near the wall, accompanied by a diffuse CH_2O cloud, indicating local quenching and incomplete oxidation. Shimizu et al. [17] examined weak flame behavior in micro-flow reactors with controlled temperature profiles. Mulla et al. [18] showed that for nearly stoichiometric flames, both the $CH_2O \cdot OH$ and $CH_2O \cdot H$ closely approximate the HRR, with $CH_2O \cdot OH$ providing a practical advantage due to more accessible detection of OH. Zhou et al. [19] employed machine learning methods to identify and construct an HRR indicator for premixed CH_4/air flames under lean-to-stoichiometric conditions. They found that the $CH_2O \cdot OH$ model is strongly influenced by the equivalence ratio and achieves high prediction accuracy near stoichiometric conditions. Chi et al. [20] performed laminar and turbulent DNS calculations for CH_4/air flames with equivalence ratios ranging from $0.6 < \Phi < 1.4$, and determined correction exponents for the investigated boundary conditions. They proposed the indicator $CH_2O^{1.17} \cdot OH^{1.07}$. Yin et al. [21] demonstrated that this approach is also applicable to the combustion of higher hydrocarbons, and showed that the $CH_2O \cdot OH$ model exhibits a good linear correlation with the HRR in turbulent spray n-heptane flames. However, numerical and experimental data across a broad range of boundary conditions, such as O_2 content in the oxidizer, preheat temperature, pressure, strain rate, and fuel-rich combustion, remain limited, highlighting a notable gap in current research. The present study aims to evaluate the validity of the $CH_2O \cdot OH$ product as a marker for HRR under these conditions. To this end, a comprehensive parametric study was carried out, spanning air to oxy-fuel combustion and systematically varying equivalence ratio, preheat temperature, pressure, and strain using multiple chemical kinetic mechanisms. The results of this study are intended to support and guide experimental diagnostics by identifying reliable marker regimes.

2. Numerical approach

In the present study, numerical calculations were carried out using the *CKReactorFreelyPropagatingFlame* solver of the ANSYS Chemkin Pro 17.0 package [22]. This program is an advanced implementation of the original *PREMIX* code developed by Kee et al. [23], and solves the 1d steady-state species and energy conservation equations governing laminar premixed planar flame. An implicit finite difference method is employed, combined with a coarse-to-fine grid refinement strategy to ensure optimal mesh distribution. The influence of strain on HRR was evaluated using the *CKReactorOpposedFlowFlame* solver, applying identical inlet conditions and fuel/oxidizer mixtures on both sides to create a symmetric twin-flame configuration. Extinction points were determined through successive approximation, following the procedure described in detail by Habisreuther et al. [24]. Typically, calculations start with an initial grid of about 10–50 points, with grid independence generally achieved between a number of 300–600 points, depending on the complexity of the chemical mechanism. Grid convergence is assessed using normalized criteria based on the maximum relative changes in species values and gradients between adjacent points, with thresholds set to 0.05 and 0.07, respectively.

In the present work, particular attention was given to the evolution of species profiles that closely resemble the spatial distribution of the HRR. As a reference, the relatively simple GRI 3.0 mechanism [25], consisting of 53 species and 325 reactions, was employed. To more accurately capture the chemistry relevant to fuel-rich flames, particularly the detailed C_2-pathways, four additional reaction mechanisms were selected: ABF [26], DLR [27], USC/II [28], and Caltech 2.3 [29,30]. These mechanisms incorporate more comprehensive higher hydrocarbon chemistry and provide improved resolution of species dynamics under fuel-rich conditions.

The study focuses on CH_4/N_2-O_2-flames, with the O_2-content in the oxidizer systematically varied from air to pure oxy-fuel conditions. To evaluate the performance of the HRR markers under diverse flame conditions, the equivalence ratio was varied over a wide range, $0.5 < \Phi < 3.3$. The inlet temperature of the fuel-oxidizer mixture was set to 300 K, 473 K, and 573 K, while the operating pressure was varied among 1 bar, 2 bar, and 5 bar. These parameters were applied to each selected chemical kinetic mechanisms, resulting in approximately 4500 computed 1d laminar freely propagating flame cases. Additionally, the influence of strain on HRR was investigated for both air and oxy-fuel flames by varying the equivalence ratio under standard inlet conditions, yielding roughly 1000 twin-flame simulations.

3. Determination of the correlation coefficient

To evaluate the strength of the association between a species-based marker and the HRR, it is essential to quantify how closely the spatial distribution of the marker reproduces the HRR profile over the entire reaction progress or an equivalent ordinate variable. The evaluation must account not only for the relative position of the HRR peak but also for the overall shape of the alignment of the profiles. The association strength between species marker and the HRR is quantified using the Pearson correlation coefficient, calculated from the spatially resolved profiles of both quantities at corresponding positions that can be experimentally obtained. Formally, the Pearson coefficient R between HRR values and

the values of an arbitrary marker M is defined as

$$R = \frac{\sum_{i=1}^{n}(HRR_i - \overline{HRR})(M_i - \overline{M})}{\sqrt{\sum_{i=1}^{n}(HRR_i - \overline{HRR})^2} \cdot \sqrt{\sum_{i=1}^{n}(M_i - \overline{M})^2}} \quad (1)$$

where HRR_i and M_i denote the ith value of the HRR and the corresponding marker quantity respectively; $\overline{HRR}$ and $\overline{M}$ represent the arithmetic mean values of their respective data series, and n is the total number of samples in each series.

To ensure that the correlation coefficient R provides a meaningful measure of the quality of the marker, a consistent and comparable ordinate basis for the profiles (e.g., the spatial flame coordinate) must be used, with sufficient resolution to weight all flame regions equally. The 1d laminar premixed flame simulations are performed on an adaptive grid, which yields a much finer, but problem-dependent, resolution in the main reaction zone. As a result, directly correlating the raw computed data would introduce bias, as the correlation would be disproportionately influenced by local variations in grid density. To mitigate this effect, the profiles were resampled at 500 equidistant points within the region relevant to heat release, defined as the spatial interval where the HRR exceeds 10% of its maximum value.

As an illustrative example, Fig. 1 demonstrates this resampling procedure for an atmospheric CH_4-air flame at an equivalence ratio $\Phi = 1.67$, preheat temperature 300 K and 1 bar. For clarity, only every 10th sampling point of the HRR and of the $CH_2O \cdot OH$ marker profile is shown. The comparison confirms that the described resampling procedure yields excellent agreement with the solution obtained from the adaptively refined grid in the flame calculations.

4. Preliminary investigations

Species commonly detected by optical diagnostics and used in the literature as markers for the HRR, either individually or in combination, include OH, CH_2O and HCO. Therefore, normalized profiles of OH, CH_2O, the product $CH_2O \cdot OH$, HCO, and the HRR are shown in Fig. 2 for a stoichiometric CH_4-air flame at standard inlet conditions, calculated using the CalTech 2.3 chemical mechanism. Among the species considered, CH_2O is formed earliest, with the onset of OH formation occurring near the CH_2O concentration peak. The product of $CH_2O \cdot OH$ exhibits a strong correlation with the HCO concentration, and both correspond well to the HRR profile. Nevertheless, a slight spatial offset between HRR and either HCO or $CH_2O \cdot OH$ is observed.

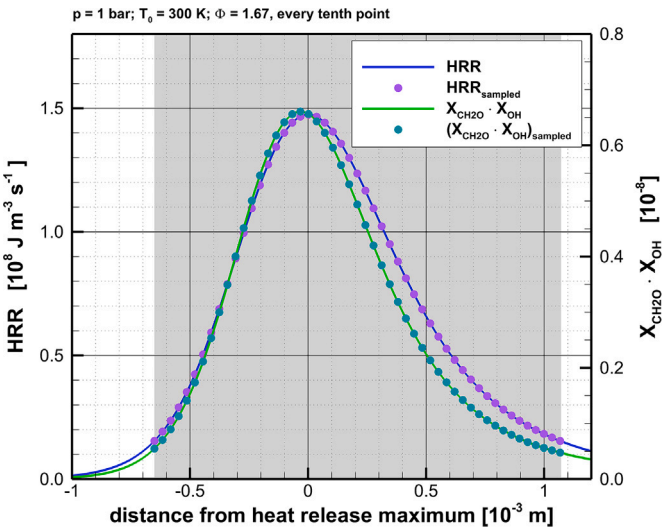

Fig. 1. Resampled profiles of heat release rate and the product of the mole fractions of CH_2O and OH as a marker.

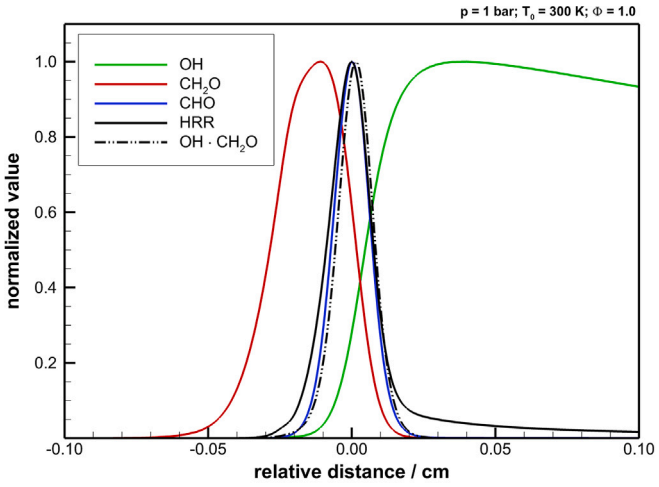

Fig. 2. Selected species and HRR of a calculated one-dimensional CH_4/air flame at $\Phi = 1.0$ (CalTech 2.3, 1 bar, 300 K).

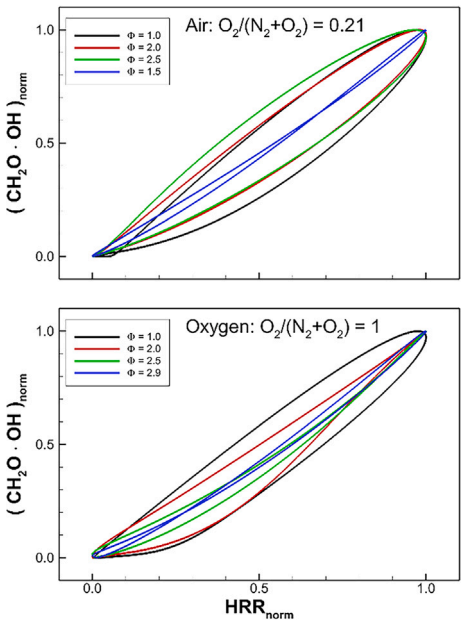

Fig. 3. Correlation between HRR and $CH_2O \cdot OH$, each normalized with their peak-value for CH_4/air and pure CH_4/O_2 at selected equivalence ratios (CalTech 2.3, 1 bar, 300 K).

Previous studies have largely focused on hydrocarbon/air flames near stoichiometric and standard conditions. To provide an initial insight into the relation between HRR and $CH_2O \cdot OH$ under oxy-fuel conditions, Fig. 3 presents a comparison of premixed CH_4/air and CH_4/O_2 flames at various equivalence ratios at standard inlet conditions. Examining the details, an almost linear correlation is observed for slightly rich CH_4-air flames at an equivalence ratio of $\Phi = 1.5$. However, the correlation quality decreases as conditions approach stoichiometric or become richer, as evidenced by the increasing scatter of the profiles. In contrast, for pure CH_4/O_2 flames, the strongest correlation occurs at ultra-rich conditions ($\Phi = 2.9$) with a gradual deterioration toward leaner mixtures. Nevertheless, in all cases, the peak of the HRR aligns closely with the peak of the $CH_2O \cdot OH$ marker.

5. Results and discussion

The following section first discusses the influence of O_2-content and equivalence ratio on the correlation between $CH_2O \cdot OH$ and HRR.

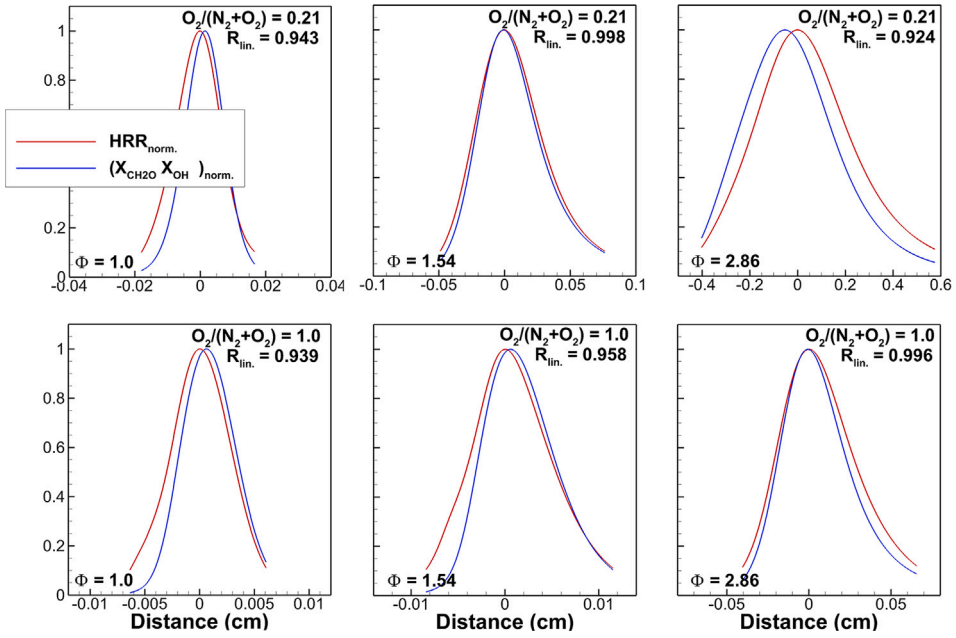

Fig. 4. $CH_2O \cdot OH$ and HRR in spatial domain for selected cases of CH_4/air- and CH_4/O_2-flames (CalTech 2.3, 1 bar, 300 K).

This is followed by an analysis of the effects of preheating and pressure, along with a comparison of results obtained using different reaction mechanisms. Finally, the impact of varying strain rates on the correlation is presented.

5.1. Influence of O_2-content and equivalence ratio

The normalized spatial distributions of the $CH_2O \cdot OH$ product and HRR are presented for selected cases in Fig. 4. The top row shows results for air combustion at standard inlet conditions, while the bottom row presents profiles for oxy-fuel combustion. For both flame types, increasing the equivalence ratio from left ($\Phi = 1.0$) to right ($\Phi = 2.86$) shifts the relative peak positions of $CH_2O \cdot OH$ and HRR. In the stoichiometric CH_4-air flame, the HRR peak precedes that of $CH_2O \cdot OH$, whereas at $\Phi = 1.5$, the peaks nearly coincide, yielding the highest correlation coefficient R. Further enrichment reverses this trend, with the $CH_2O \cdot OH$ peak appearing before the HRR peak and a corresponding decline in correlation. A similar behavior is observed in oxy-fuel flames, although the best overlap, and hence the strongest correlation, occurs at higher equivalence ratios ($\Phi = 2.9$). To complement the initial visual assessment, the Pearson correlation coefficient R is presented in Fig. 5. Across the entire range of conditions examined, high correlation values ($R > 0.9$) are observed, demonstrating the generally strong performance of $CH_2O \cdot OH$ as a marker for HRR. A comparison between Figs. 4 and 5 indicates that only in cases where $R > 0.98$ does $CH_2O \cdot OH$ accurately reproduce both the shape and the peak position of the HRR profile without any noticeable spatial shifts. For CH_4–air combustion, such high correlations are limited to narrow ranges around $\Phi = 0.5$ and $\Phi = 1.5$. In contrast, oxy-fuel flames show the lowest correlation at lean conditions ($\Phi = 0.65$), while R increases steadily with richer mixtures, reaching a maximum at $\Phi = 3.0$. It should be mentioned that in fuel-rich (oxy-fuel) flames, two distinct HRR zones can be identified: a primary positive zone, which drives a strong temperature rise, followed by a negative zone after the temperature peak. The latter reflects endothermic reactions and the formation of syngas (H_2 and CO). Nevertheless, the major exothermic heat release is locally decoupled from these slower endothermic processes (especially in the case of oxy-fuel), leading to so-called super-adiabatic flame temperatures. Near-stoichiometric conditions are characterized by elevated radical pool concentrations, particularly of H, O, and OH,

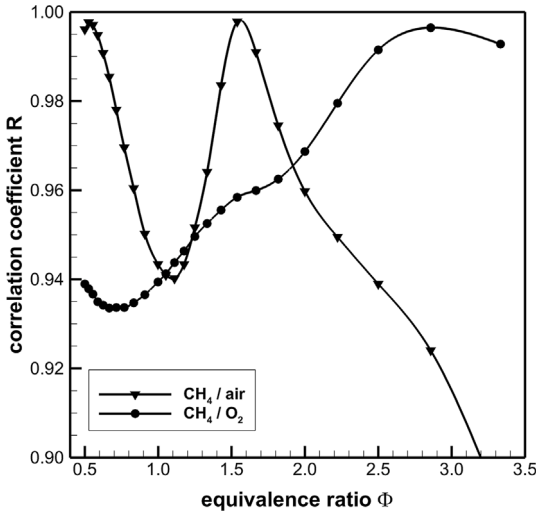

Fig. 5. Pearson correlation coefficient of $CH_2O \cdot OH$ vs. HRR for CH_4/air and CH_4/O_2) varying equivalence ratio (CalTech 2.3, 1 bar, 300 K).

resulting from enhanced thermal dissociation at flame temperatures approaching 3000 K [31], which may influence the correlation.

5.2. Influence of preheating and pressure

Preheating and elevated pressure significantly influence reaction pathways and can affect the validity of $CH_2O \cdot OH$ as an HRR marker. Fig. 6 presents the Pearson correlation coefficient R as a function of equivalence ratio for both air and oxy-fuel flames under these conditions. Overall, the general shape of the correlation profiles remains consistent across different thermodynamic states. For air combustion, high correlation coefficients are observed in two distinct equivalence ratio ranges around $\Phi = 0.5$ and $\Phi = 1.5$, with a reduction near stoichiometric conditions. In oxy-fuel flames, the strongest correlation occurs in the ultra-rich regime near $\Phi = 3.0$, decreasing toward lean and stoichiometric mixtures. Preheating shifts the correlation profiles toward

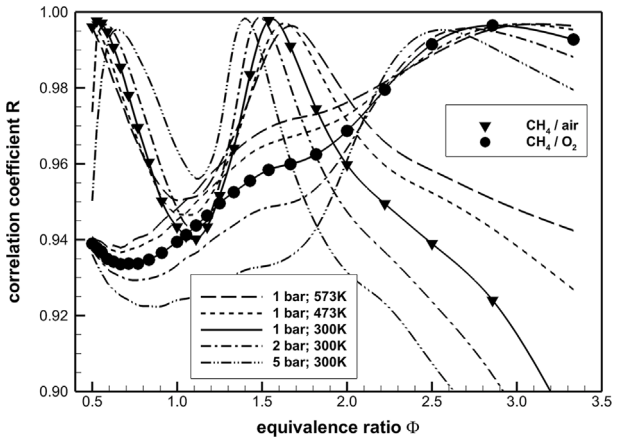

Fig. 6. Pearson correlation coefficient of HRR vs. $CH_2O \cdot OH$ for CH_4/air and CH_4/O_2 varying equivalence ratio (CalTech 2.3, 1 bar, 300 K).

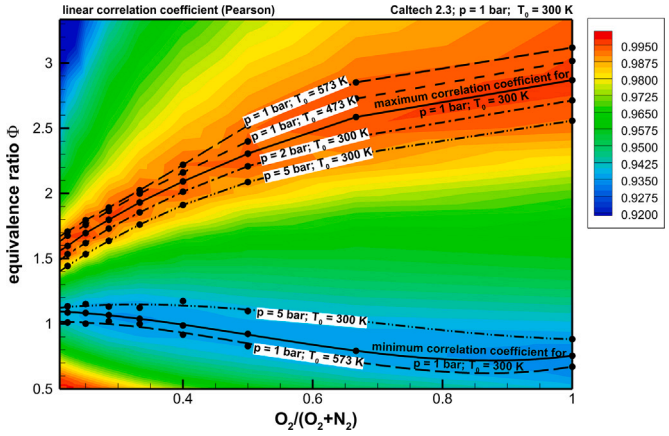

Fig. 7. Pearson correlation coefficient (coloured legend) depending on equivalence ratio and O_2-content (CalTech 2.3, varying inlet conditions).

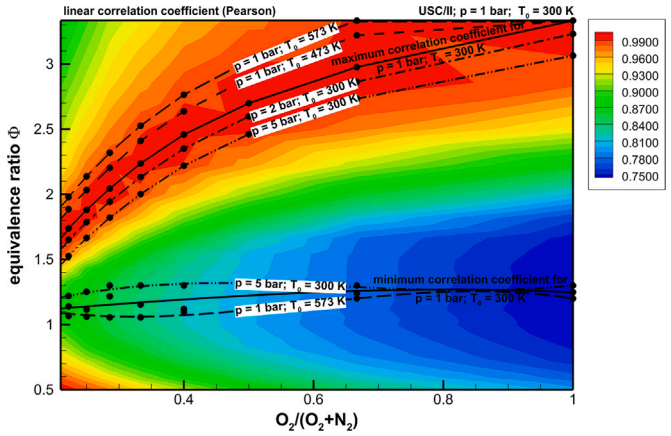

Fig. 8. Pearson correlation coefficient (coloured legend) depending on equivalence ratio and O_2-content (USC/II, varying inlet conditions).

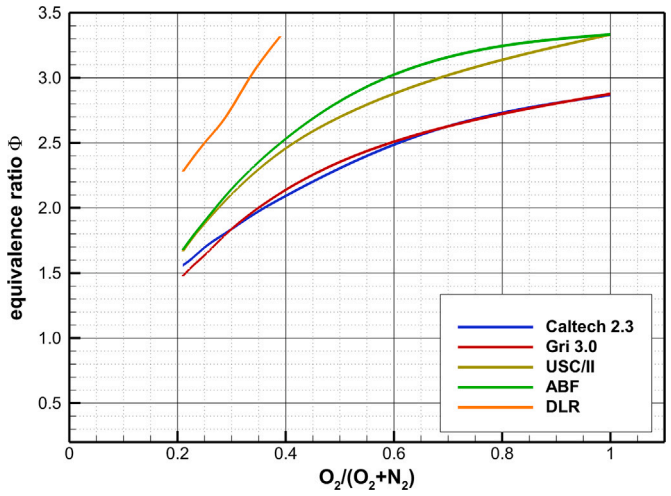

Fig. 9. Equivalence ratio with maximum Pearson correlation coefficient depending on O_2-content calculated with different mechanism (1 bar, 300 K).

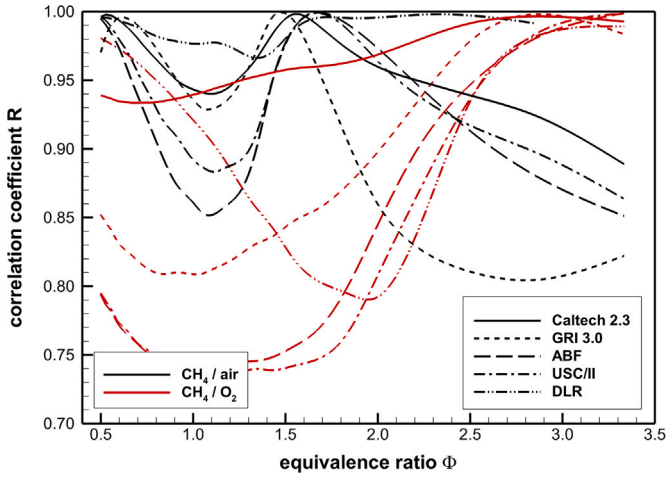

Fig. 10. Comparison of the quantity of the correlation coefficient for different mechanism (1 bar, 300 K).

higher equivalence ratios, while elevated pressure shifts them toward lower equivalence ratios. Notably, near-stoichiometric oxy-fuel flames exhibit a decrease in R under elevated pressure, contrasting with the trends in air flames. The full set of simulated flame cases is summarized in Fig. 7 as a color map of R, with overlaid lines indicating the lean-side maxima and rich-side minima of the correlation coefficient for each thermodynamic condition. These results highlight how thermodynamic effects modulate the reliability of $CH_2O \cdot OH$ as an HRR marker across different flame regimes.

5.3. Reaction mechanisms

Fig. 8 shows the correlation coefficient map obtained using the USC/II mechanism. Overall trends are similar to those obtained with the CalTech 2.3 mechanism (Fig. 7), with maximum correlation coefficients occurring at higher equivalence ratios, while minima remain near stoichiometric conditions. The equivalence ratio corresponding to the highest correlation depends on the O_2 content in the oxidizer and is summarized in Fig. 9 for various chemical mechanisms under standard conditions. GRI 3.0 and CalTech 2.3 predict an increase from $\Phi = 1.5$ in air flames to $\Phi = 2.9$ in pure oxy-fuel flames, with nearly identical results, whereas ABF and USC/II show a shift to higher equivalence ratios ($\Phi = 1.7$ to 3.3). The DLR mechanism exhibits particularly strong correlation in oxygen-enriched, fuel-rich flames. For a comprehensive comparison, Fig. 10 presents R as a function of equivalence ratio for all mechanisms, covering both air and oxy-fuel combustion. Preheating and elevated pressure shift the correlation profiles consistently across mechanisms, following the trends described previously. In addition to trends, the absolute values of R vary with the reaction mechanism. This effect is

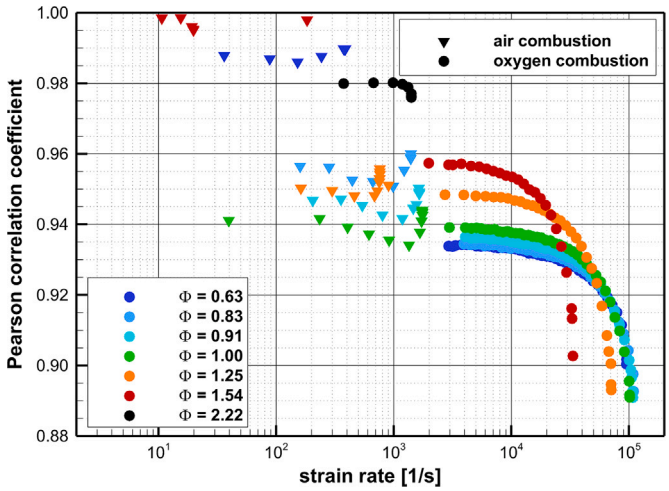

Fig. 11. Pearson correlation coefficient depending on the strain rate for CH_4/air and CH_4/O_2 varying equivalence ratio (CalTech 2.3, 1 bar, 300 K).

particularly pronounced in oxy-fuel flames, where ABF and USC/II yield the lowest correlation near stoichiometric conditions ($R \approx 0.73$), while CalTech 2.3 provides the highest values. All mechanisms predict a maximum correlation R_{max} at $\Phi = 3.0$ for oxy-fuel flames. For CH_4–air flames, all mechanisms display two local maxima at approximately $\Phi = 0.5$ and $\Phi = 1.5$, respectively.

5.4. Influence of strain

Resistance to extinction under stretch is a key characteristic of flames, particularly under turbulent conditions [32]. To evaluate the behavior of $CH_2O \cdot OH$ under such conditions, selected cases were simulated in an opposed-flow configuration, with the strain rate incrementally increased until flame extinction. Fig. 11 shows the resulting Pearson correlation coefficient as a function of strain rate for premixed CH_4/air and CH_4/O_2 flames, calculated using the CalTech 2.3 mechanism, with strain rate defined by the maximum velocity gradient upstream of the flame front. The results indicate that $CH_2O \cdot OH$ remains a robust marker for HRR at strain rates relevant to technical applications (<10,000 s^{-1}). Near stoichiometric conditions ($0.84 < \Phi < 1.25$), correlation values are similar for both air and oxy-fuel flames. For CH_4/air, R slightly increases as extinction is approached, while CH_4/O_2 flames show a noticeable decrease. Overall, these findings confirm the applicability of $CH_2O \cdot OH$ as an HRR marker even under high-strain conditions typical of turbulent combustion.

5.5. Conclusion

The results demonstrate that high-temperature HRR can be accurately captured using the marker $CH_2O \cdot OH$. For CH_4–air flames, the highest correlation occurs under slightly rich conditions at $\Phi = 1.5$, with a secondary maximum around $\Phi \approx 0.5$ in the lean regime. For rich CH_4/O_2 flames, the strongest correlation is observed between $2.5 < \Phi < 3.0$, while near-stoichiometric conditions consistently show lower correlation. Preheating broadens the range of equivalence ratios over which $CH_2O \cdot OH$ is a reliable marker, whereas elevated pressure shifts the optimal range toward leaner mixtures and narrows the domain of high correlation. Although increasing strain reduces R, it remains approximately 0.9 near extinction, confirming the robustness of $CH_2O \cdot OH$ even under highly turbulent conditions. Beyond these numerical findings, the results are intended to support and guide experimental diagnostics by identifying reliable marker regimes.

CRediT authorship contribution statement

Björn Stelzner: Writing – review & editing, Writing – original draft, Investigation, Formal analysis, Conceptualization. **Peter Habisreuther:** Writing – review & editing, Writing – original draft, Visualization, Investigation, Formal analysis, Conceptualization. **Fabian P. Hagen:** Writing – review & editing, Investigation, Conceptualization. **Matthias M. Sentko:** Writing – review & editing, Investigation, Conceptualization. **George Vourliotakis:** Writing – review & editing, Investigation, Conceptualization. **Christos Keramiotis:** Writing – review & editing, Investigation, Conceptualization. **Maria Founti:** Writing – review & editing, Supervision, Resources. **Dimosthenis Trimis:** Writing – review & editing, Supervision, Resources.

Declaration of competing interest

The authors declare that they have no known competing financial interests or personal relationships that could have appeared to influence the work reported in this paper.

Acknowledgment

The present research work contributes to the MTET program, Resource and Energy Efficiency, Anthropogenic Carbon Cycle (38.05.01) of Helmholtz Association.

Data availability

Data will be made available on request.

References

[1] Najm HN, Paul PH, Mueller CJ, Wyckoff PS. On the adequacy of certain experimental observables as measurements of flame burning rate. Combust Flame 1998;113(3):312–32. https://doi.org/10.1016/S0010-2180(97)00209-5

[2] Jeffries JB, Crosley DR, Wysong IJ, Smith GP. Laser-induced fluorescence detection of HCO in a low-pressure flame. Symp Int Combust 1991;23(1):1847–54, Twenty-Third Symposium (International) on Combustion. doi:https://doi.org/10.1016/S0082-0784(06)80465-0. https://www.sciencedirect.com/science/article/pii/S0082078406804650.

[3] Kiefer J, Li ZS, Seeger T, Leipertz A, Aldén M. Planar laser-induced fluorescence of HCO for instantaneous flame front imaging in hydrocarbon flames. Proc Combust Inst 2009;32(1):921–8. https://doi.org/10.1016/j.proci.2008.05.013. https://www.sciencedirect.com/science/article/pii/S1540748908000667.

[4] Zhou B, Kiefer J, Zetterberg J, Li Z, Aldén M. Strategy for PLIF single-shot HCO imaging in turbulent methane/air flames. Combust Flame 2014;161(6):1566–74. https://doi.org/10.1016/j.combustflame.2013.11.019

[5] Paul PH, Najm HN. Planar laser-induced fluorescence imaging of flame heat release rate. Symp Int Combust 1998;27(1):43–50, twenty-Seventh Sysposium (International) on Combustion Volume One. doi:https://doi.org/10.1016/S0082-0784(98)80388-3. https://www.sciencedirect.com/science/article/pii/S0082078498803883.

[6] Böckle S, Kazenwadel J, kunzelmann T, Shin D-I, Schulz C, Wolfrum J. Simultaneous single-shot laser-based imaging of formaldehyde, OH, and temperature in turbulent flames. Proc Combust Inst 2000;28(1):279–86. https://doi.org/10.1016/S0082-0784(00)80221-0. https://www.sciencedirect.com/science/article/pii/S0082078400802210.

[7] Gordon RL, Masri AR, Mastorakos E. Heat release rate as represented by [OH] × [CH_2O] and its role in autoignition. Combust Theory Model 2009;13(4):645–70. https://doi.org/10.1080/13647830902957200

[8] Röder M, Dreier T, Schulz C. Simultaneous measurement of localized heat-release with OH/CH_2O–LIF imaging and spatially integrated OH* chemiluminescence in turbulent swirl flames. Proc Combust Inst 2013;34(2):3549–56. https://doi.org/10.1016/j.proci.2012.06.102. https://www.sciencedirect.com/science/article/pii/S1540748912002106.

[9] Xin S, Yang F, Wang X, He Y, Weng W, Wang Z. Effects of H_2 enrichment on combustion characteristics in inverse swirl diffusion flames of H_2-doped jet fuel using OH, CH_2O, fuel and temperature imaging. Fuel 2024;369:131704. https://doi.org/10.1016/j.fuel.2024.131704. https://www.sciencedirect.com/science/article/pii/S0016236124008524.

[10] Retzer U, Pan R, Werblinski T, Huber FJT, Slipchenko MN, Meyer TR, Zigan L, Will S. Burst-mode OH/CH_2O planar laser-induced fluorescence imaging of the heat release zone in an unsteady flame. Opt Express 2018;26(14):18105–14. https://doi.org/10.1364/OE.26.018105. https://opg.optica.org/oe/abstract.cfm?URI=oe-26-14-18105.

[11] Osborne JR, Ramji SA, Carter CD, Peltier S, Hammack S, Lee T, Steinberg AM. Simultaneous 10 khz TPIV, OH PLIF, and CH_2O PLIF measurements of turbulent flame structure and dynamics. Exp Fluids 2016;57(5):65. https://doi.org/10.1007/s00348-016-2151-7

[12] Vena PC, Deschamps B, Guo H, Smallwood GJ, Johnson MR. Heat release rate variations in a globally stoichiometric, stratified iso-octane/air turbulent V-flame. Combust Flame 2015;162(4):944–59. https://doi.org/10.1016/j.combustflame.2014.09.019. https://www.sciencedirect.com/science/article/pii/S0010218014003009.
[13] Wei ZL, Leung CW, Cheung CS, Huang ZH. Single-valued prediction of markers on heat release rate for laminar premixed biogas-hydrogen and methane-hydrogen flames. Energy 2017;133:35–45. https://doi.org/10.1016/j.energy.2017.05.112. https://www.sciencedirect.com/science/article/pii/S036054421730868X.
[14] Singh G, Juddoo M, Kourmatzis A, Dunn MJ, Masri AR. Heat release zones in turbulent, moderately dense spray flames of ethanol and biodiesel. Combust Flame 2020;220:298–311. https://doi.org/10.1016/j.combustflame.2020.07.005. https://www.sciencedirect.com/science/article/pii/S0010218020302674.
[15] Kosaka H, Zentgraf F, Scholtissek A, Hasse C, Dreizler A. Effect of flame-wall interaction on local heat release of methane and DME combustion in a side-wall quenching geometry. Flow Turbul Combust 2020;104(4):1029–46. https://doi.org/10.1007/s10494-019-00090-4
[16] Fan L, Savard B, Fond B, Durocher A, Bergthorson J, Carlyle S, Vena P. Mechanisms leading to stabilization and incomplete combustion in lean CH_4/H_2 swirling wall-impinging flames. J Eng Gas Turbines Power 2024;146(6):061015. https://doi.org/10.1115/1.4063833. https://asmedigitalcollection.asme.org/gasturbinespower/article-pdf/146/6/061015/7227202/gtp_146_06_061015.pdf.
[17] Shimizu T, Nakamura H, Tezuka T, Hasegawa S, Maruta K. OH and CH_2O laser-induced fluorescence measurements for hydrogen flames and methane, N-butane, and dimethyl ether weak flames in a micro flow reactor with a controlled temperature profile. Energy Fuels 2017;31(3):2298–307. https://doi.org/10.1021/acs.energyfuels.6b02325
[18] Mulla IA, Dowlut A, Hussain T, Nikolaou ZM, Chakravarthy SR, Swaminathan N, Balachandran R. Heat release rate estimation in laminar premixed flames using laser-induced fluorescence of CH_2O and h-atom. Combust Flame 2016;165:373–83. https://doi.org/10.1016/j.combustflame.2015.12.023. https://www.sciencedirect.com/science/article/pii/S0010218015004666.
[19] Zhou T, Tang P, Ye T. Machine learning based heat release rate indicator of premixed methane/air flame under wide range of equivalence ratio. Energy 2023;263:126103. https://doi.org/10.1016/j.energy.2022.126103. https://www.sciencedirect.com/science/article/pii/S0360544222029899.
[20] Chi C, Janiga G, Zähringer K, Thévenin D. DNS study of the optimal heat release rate marker in premixed methane flames. Proc Combust Inst 2019;37(2):2363–71. https://doi.org/10.1016/j.proci.2018.07.095. https://www.sciencedirect.com/science/article/pii/S1540748918305133.
[21] Yin Y, Gong X, Zhou H, Ren Z. The correlation of species concentration with heat release rate in an auto-igniting turbulent n-heptane spray flame. Fuel 2020;262:116510. https://doi.org/10.1016/j.fuel.2019.116510. https://www.sciencedirect.com/science/article/pii/S0016236119318642.
[22] Reaction Design. ANSYS chemkin theory manual 17.0 (15151). San Diego: ANSYS Inc.; 2015.
[23] Kee RJ, Rupley FM, Miller JA. CHEMKIN-II: a fortran chemical kinetics package for the analysis of gas phase chemical kinetics, Technical Report SAND89-8009B, Sandia National Laboratories; 1989.
[24] Habisreuther P, Stelzner B, Loukou A, Vlavakis P, Trimis D. Structure transition from oxygen-enhanced to oxy-fuel methane non-premixed flames near extinction. Fuel 2019;239:357–64. https://doi.org/10.1016/j.fuel.2018.11.028
[25] Smith GP, Golden DM, Frenklach M, Moriarty NW, Eiteneer B, Goldenberg M, Bowman CT, Hanson RK, Song S, Jr. WCG, Lissianski VV, Qin Z. GRI-mech 3.0; 2000. http://combustion.berkeley.edu/gri-mech/releases.html [accessed: 1 March 2025].
[26] Appel J, Bockhorn H, Frenklach M. Kinetic modeling of soot formation with detailed Chemistry and physics: laminar premixed flames of C_2 hydrocarbons. Combust Flame 2000;121(1):122–36. https://doi.org/10.1016/S0010-2180(99)00135-2. https://www.sciencedirect.com/science/article/pii/S0010218099001352.
[27] Chernov V, Thomson MJ, Dworkin SB, Slavinskaya NA, Riedel U. Soot formation with C_1 and C_2 fuels using an improved chemical mechanism for PAH growth. Combust Flame 2014;161(2):592–601. https://doi.org/10.1016/j.combustflame.2013.09.017. https://www.sciencedirect.com/science/article/pii/S0010218013003490.
[28] Wang H, You X, Joshi AV, Davis SG, Laskin A, Egolfopoulos F, Law CK. USC mech version II; 2007. http://ignis.usc.edu/USC_Mech_II.htm [accessed: 1 March 2025].
[29] Narayanaswamy K, Blanquart G, Pitsch H. A consistent chemical mechanism for oxidation of substituted aromatic species. Combust Flame 2010;157(10):1879–98. https://doi.org/10.1016/j.combustflame.2010.07.009. https://www.sciencedirect.com/science/article/pii/S0010218010001975.
[30] Blanquart G. Effects of spin contamination on estimating bond dissociation energies of polycyclic aromatic hydrocarbons. Int J Quantum Chem 2015;115(12):796–801. https://doi.org/10.1002/qua.24904. https://onlinelibrary.wiley.com/doi/pdf/10.1002/qua.24904.
[31] Stelzner B, Weis C, Habisreuther P, Zarzalis N, Trimis D. Super-adiabatic flame temperatures in premixed methane flames: a comparison between oxy-fuel and conventional AIR combustion. Fuel 2017;201:148–55. https://doi.org/10.1016/j.fuel.2017.01.025
[32] Long AE, Burbano H, Speth RL, Movaghar A, Egolfopoulos FN, Green WH. An apparatus-independent extinction strain rate in counterflow flames. Proc Combust Inst 2019;37(2):1979–87. https://doi.org/10.1016/j.proci.2018.06.130. https://www.sciencedirect.com/science/article/pii/S1540748918303134.